Liu, Tao; Yuan, Jiashu; Zhen, Yihan; Zhang, Cuijuan; Li, Yongdan

Porous poly(vinylidene fluoride) (PVDF) membrane with 2D vermiculite nanosheets modification for non-aqueous redox flow batteries

Published in:
Journal of Membrane Science

DOI:
10.1016/j.memsci.2022.120468

Published: 05/06/2022

Document Version
Peer-reviewed accepted author manuscript, also known as Final accepted manuscript or Post-print

Porous poly(vinylidene fluoride) (PVDF) membrane with 2D vermiculite nanosheets modification for non-aqueous redox flow batteries

Tao Liu[a,b], *Jiashu Yuan*[a,b,c], *Yihan Zhen*[a,b], *Cuijuan Zhang*[*a,b], *Yongdan Li*[a,b,c]

[a] State Key Laboratory of Chemical Engineering, Tianjin Key Laboratory of Applied Catalysis Science and Technology, School of Chemical Engineering and Technology, Tianjin University, Tianjin 300072, China. Email: cjzhang@tju.edu.cn

[b] Collaborative Innovation Center of Chemical Science and Engineering (Tianjin), Tianjin 300072, China

[c] Department of Chemical and Metallurgical Engineering, School of Chemical Engineering, Aalto University, Kemistintie 1, Espoo, P.O. Box 16100, FI-00076, Aalto, Finland.

Abstract

Lack of high-performance membrane seriously limits the performance of non-aqueous redox flow batteries (NARFBs). Here, a porous poly(vinylidene fluoride) (PVDF) membrane with 2D vermiculite nanosheets modification is proposed and prepared. The vermiculite nanosheets act as barriers to alleviate the crossover of active species. The hydrogen bonding between vermiculite and PVDF skeleton effectively mitigates the swelling rate and increases the mechanical strength of the membrane. The resultant battery constructed with the new porous membrane exhibits higher Coulombic efficiency (97.9% vs 84.6%) and large average discharge capacity (0.132 vs 0.088 Ah L^{-1}) compared with the one with pristine PVDF membrane at 2 mA cm^{-2}. The vermiculite nanosheets have little effect on the voltage efficiency (90.6% vs 92.7%).

Keywords: non-aqueous redox flow battery; porous membrane; vermiculite nanosheets; PVDF

1. Introduction

Redox flow battery (RFB) is a promising grid-scale energy storage device for the employment of renewable but intermittent solar and wind energy owing to its unique characteristics [1,2]. Based on the solvent used (water or organic solvents), RFB can be divided into aqueous RFB (ARFB) and non-aqueous RFB (NARFB), the latter possess higher energy density due to the wider electrochemical window [3]. Since Matsuda et al. designed the first NARFB using ruthenium complex $[Ru(bpy)_3](BF_4)_2$ [4], increasing efforts have been devoted to developing NARFBs [5]. However, no commercial NARFBs have been demonstrated yet.

Among the various challenges, the membrane, as an important component, has serious crossover effect, which significantly limits the performance of NARFBs. Although many membranes have been used in NARFBs [6], almost all of them are just transferred from other technologies such as lithium-ion battery, none is specially designed for NARFBs. In addition, the active materials for NARFBs generally have low solubility, the active materials and/or their charged/discharged species can precipitate and deposit on the membrane, which further aggregates the battery performance [7,8]. Accordingly, it is greatly desirable to develop advanced membrane for NARFBs.

The porous membrane has been designed for RFBs considering the high ion conductivity, good chemical stability and cost-effectiveness [9]. Zhang and his colleagues proposed and designed nanofiltration membranes with tunable pore size distribution [10,11]. The polyacrylonitrile (PAN)-based membrane showed improved ion selectivity from 6.9 to 14.9. The resultant vanadium-based RFB (VRB) performance is comparable to that of Nafion 117 but at much lower cost. Che et al. developed porous

polybenzimidazole (PBI) membrane by hard templating method [12]. The area resistance and vanadium ion permeability of the membrane were significantly reduced while the efficiency of the battery was obviously enhanced. A polymer of intrinsic microporosity membrane with pore sizes of 0.4–0.8 nm was prepared for NARFB, which delivers impressive Coulombic efficiency (CE) of 95% over 6 days [13]. As a mechanically strong, thermally stable, chemically corrosion resistant, and hydrophobic membrane [14], the poly(vinylidene fluoride) (PVDF) membrane has been widely used [15,16]. Wei et al. firstly investigated the PVDF ultrafiltration membrane in VRB application and found that the ion selectivity can be tuned readily by adjusting the preparation parameters. The battery with 125 μm thick membrane showed Coulombic efficiency (CE) of 95% and energy efficiency (EE) of 78.6% [17]. However, those porous membranes show very high swelling in organic solvents, leading to rapid diffusion of active materials and capacity degradation, which is a great challenge for NARFB. Furthermore, the crossover effect is serious for porous membranes due to their generally larger pore size [18]. Correspondingly, strategies have to be developed to improve the performance of existed porous membrane or design new porous membrane for NARFBs.

Introducing inorganic nanoparticles has been proved effective to modify the porous membranes. The chemically stable inorganic nanoparticles introduced into the membrane can effectively reduce the pore size and thus alleviate the diffusion of active species. Furthermore, the interaction between the nanoparticle filler and the polymer framework of the membrane effectively mitigates the swelling rate and improves the mechanical properties [19-21]. The 2D materials provide an alternative to reduce the diffusion of active materials considering their large surface area and low thickness, which is

demonstrated in our recent work on Ni-metal organic framework nanosheets [22]. Similar results have been reported for graphene [23], MoS_2 [24], and SiC [25] nanosheets. Vermiculite, a layered silicate, can be peeled into nanosheets by many methods [26] and have been used in batteries [27,28]. We recently loaded layers of vermiculite nanosheets on the surface of porous membrane to reduce the diffusion of active species [29]. The resultant battery showed improved performance in terms of higher CE. However, since the vermiculite layer with small pores is a physical layer on the porous substrate, serious deposition of the active specie is found, which is harmful for the battery cycling stability. Herein, we designed an intrinsic membrane [18] specially for NARFBs, porous PVDF membrane with 2D vermiculite nanosheets embedded. The 2D vermiculite nanosheets were added into the PVDF casting solution as fillers during preparation. They can effectively reduce the swelling and increase the mechanical strength of the membrane. The intrinsic membrane with the vermiculite nanaosheets can effectively suppress the crossover of the active species and more importantly, shows no deposition of the active species, which contribute to high CE and cycling stability.

2. Experimental

2.1. Membrane preparation

The preparation and characterization details of 2D vermiculite nanosheets can be found in our previous work [29]. The vermiculite film, obtained from the exfoliated vermiculite (Xinjiang, China) colloid solution, was re-dispersed in N,N-dimethylformamide (DMF, 99.5%, Greagent) by ultrasound for 2 h to obtain the vermiculite-DMF colloid for later use. The 2D vermiculite nanosheets modified PVDF (HSV-900, Kynar) membranes were prepared by the immersion precipitation phase

inversion method. 2, 4, 8 and 16 g of vermiculite-DMF colloid was added into DMF to prepare 20 g mixed solution (the mass percentage of vermiculite nanosheets to PVDF is 0.043 wt%, 0.085 wt%, 0.17 wt% and 0.34 wt%, respectively), followed by ultrasonication for 20 min. 3 g of PVDF powder was then added, which was fully dissolved at 75 ºC for 24 h. The resultant solution was coated on a glass plate with a scraper. After standing in room temperature air for 30 s, the coated glass plate was transferred to a deionized water coagulation bath for solvent exchange. After soaking in water for 24 h, the membrane was dried at 60 ºC for 48 h, which were denoted as Vrm@PVDF-0.034wt%, Vrm@PVDF-0.085wt%, Vrm@PVDF-0.17wt% and Vrm@PVDF-0.34wt%, respectively. The pristine PVDF membrane (PVDF) was prepared by the similar procedure except without vermiculite-DMF colloid.

2.2. Electrochemical test

The flow battery performance was tested with an in-house designed flow battery system in the argon-filled glove box by the LAND test system with flowing electrolytes (30 ml min^{-1}). N-(ferrocenylmethyl)-N,N-dimethyl-N-ethylammonium bis (trifluoromethane-sulfonyl) imide (Fc1N112-TFSI) and tetraethylammonium bis(trifluoromethylsulfonyl) imide (TEATFSI) were synthesized following the reported procedure [30,31]. Fc1N112-TFSI/TEATFSI/acetonitrile (MeCN, 99.9%, Sigma-Aldrich) and $Fe(acac)_3$/TEATFSI/MeCN were employed as catholyte (10 mL) and anolyte (10 mL), respectively. The electrochemical impedance spectra (EIS) were collected on the electrochemical station (VersaSTAT3, Princeton Applied Research, USA) over 10^6–0.1 Hz with a perturbation amplitude of 10 mV.

2.3. Other characterization

The porous membranes were cut into 5 × 1 cm long strips and soaked in acetonitrile for 24 h, then the length change was measured. The swelling rate (*SR*) is calculated according to eq. (1):

$$SR = \frac{L_{wet} - L_{dry}}{L_{wet}} \times 100\% \quad (1)$$

where L_{dry} and L_{wet} are the length of dry and wet membranes, respectively.

The porous membranes were cut into 2 × 1 cm long strips, which were stretched at a constant speed of 10 mm min^{-1} by a microtester (Instron 5848, Britain). The breaking strength is calculated according to eq. (2):

$$\text{Breaking strength} = \frac{F}{S} \times 100\% \quad (2)$$

where *F* is the maximum force at the point of sample breaking, *S* the cross-sectional area of sample.

The surface and cross-section microstructures of pristine and modified PVDF films were observed by scanning electron microscope (SEM, FEI, America) equipped with an energy dispersive spectroscopy (EDS) unit for elemental mapping. The films were treated in liquid nitrogen to prepare samples for microstructure observation. The pore properties of the membranes, degassed at 60 °C for 12 h, were measured with an absorption apparatus (Autosorb-1, Quantachrome, America) by the nitrogen sorption analysis at 77 K. The macropore size distribution was tested through mercury intrusion porosimetry (Micromeritics AutoPore 9520). Thermal gravimetric analysis (TGA) was tested (TA Instruments Netzsch STA 449C) at a heating rate of 10 °C min^{-1} in N_2 atmosphere to evaluate the thermal stability of the membranes. The permeability of the membranes was tested with an H-cell, the details are provided in our recent work [22].

3. Results and discussion

The membranes were prepared by immersion precipitation phase inversion method, as schematically illustrated in Scheme 1. The 2D vermiculite nanosheets were prepared by ionic exchange method [29]. The surface of PVDF membrane is loose and porous (Fig. 1a) with finger-like pores in the cross-section (Fig. 1c), which are the typical microstructures of samples prepared by the phase-inversion method. After adding 2D vermiculite nanosheets, the surface (Fig. 1b) becomes dense, and the finger-like pores disappear although the membrane is still porous (Fig. 1d). It is noted that the porosity decreases with the content of vermiculite nanosheets (not shown here). The strong interaction between vermiculite nanosheets and PVDF probably slows down the solvent erosion rate during solvent exchange, leading to denser structures and smaller pores. Such denser structure is expected to inhibit the diffusion of active species during battery cycling. The surface EDS elemental mapping (Fig.1e) show that the vermiculite in the Vrm@PVDF membrane maintains its 2D nanosheet characteristics, which can reduce the diffusion of active materials. The cross-section EDS elemental mapping (Fig. 1f) demonstrates the uniform distribution of vermiculite nanosheets throughout the separator.

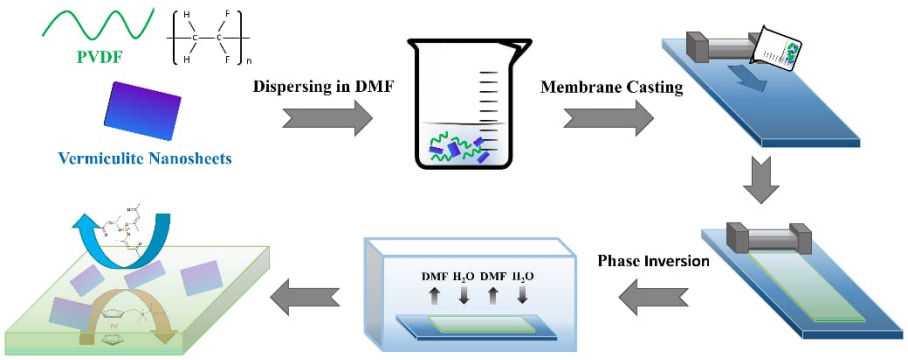

Scheme 1. Illustration of the preparation procedure of Vrm@PVDF membrane.

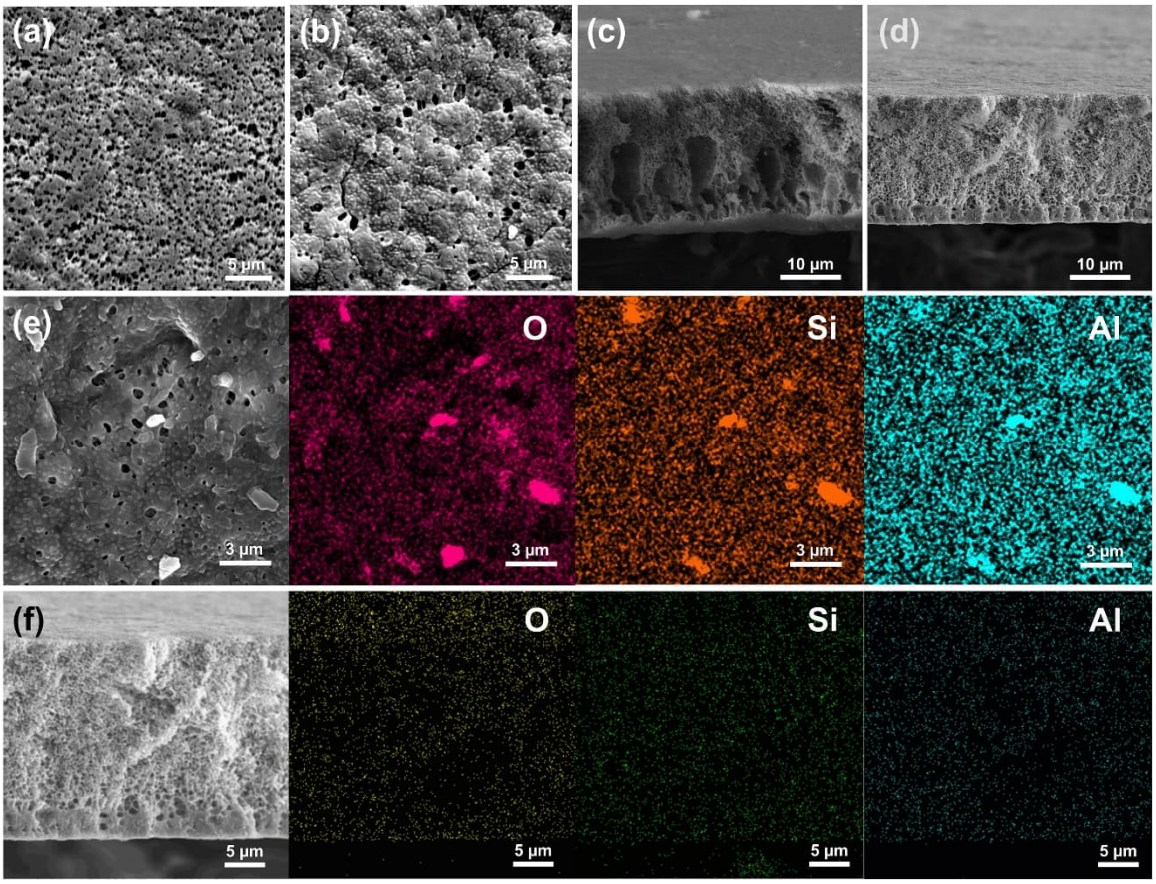

Fig. 1. (a, b) surface and (c, d) cross-section SEM images of PVDF (a, c) and Vrm@PVDF-0.17wt% porous membrane (b, d). (e) Surface and (f) cross-section EDS elemental mapping of Vrm@PVDF-0.17wt%.

The swelling ratio is an important metrics of porous membrane. Swelling will aggravate the permeation of the active materials and also reduce the mechanical properties of membrane [32]. The addition of vermiculite nanosheets can effectively reduce the swelling of PVDF membrane in acetonitrile, as the swelling ratio decreases with the content of vermiculite nanosheets (Fig. 2a). Simultaneously, the tensile strength of membranes increases. The hydroxyl group on the surface of vermiculite forms a strong hydrogen bond with the fluorine atom of PVDF, which makes the polymer framework more compact and resistant to swelling and breaking [33-35]. The TGA results in N_2

atmosphere (Fig. 2b) show that both PVDF and Vrm@PVDF-0.17wt% membranes exhibit no weight loss before 400 ºC. The temperature at which the weight starts to lose is higher for the Vrm@PVDF-0.17wt% membrane, which indicates that the addition of vermiculite nanosheets can improve the thermal stability of the PVDF membranes.

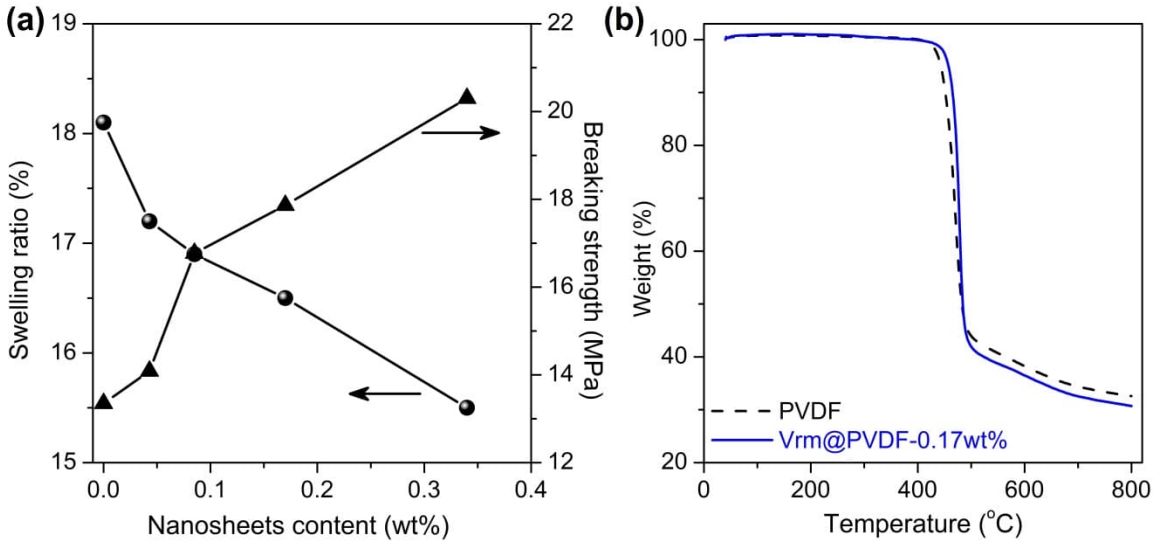

Fig. 2. (a) Swelling ratio and mechanical properties, and (b) thermal stability of pristine and modified PVDF membranes.

The pore properties of PVDF and Vrm@PVDF-0.17wt% membranes were examined by nitrogen sorption. PVDF and Vrm@PVDF-0.17wt% porous membranes exhibit similar isothermal curve and hysteresis loop (Fig. 3a), which belong to type II and type IV mixed isotherms, indicating the coexistence of macropores and mesopores. The Barret-Joyner-Halenda (BJH) pore size distribution (Fig. 3b) is similar, with pores centering at ~20 nm. The addition of vermiculite nanosheets has limited effect on the size of mesopores but the amount of mesopores decreases. The mercury intrusion porosimetry test reveals that the amount of macropores of 0.1-1 μm declines and the pore sizes

become smaller (Fig. 3c) probably due to the filling of the vermiculite nanosheets in the finger-like pores, in agreement with the SEM results.

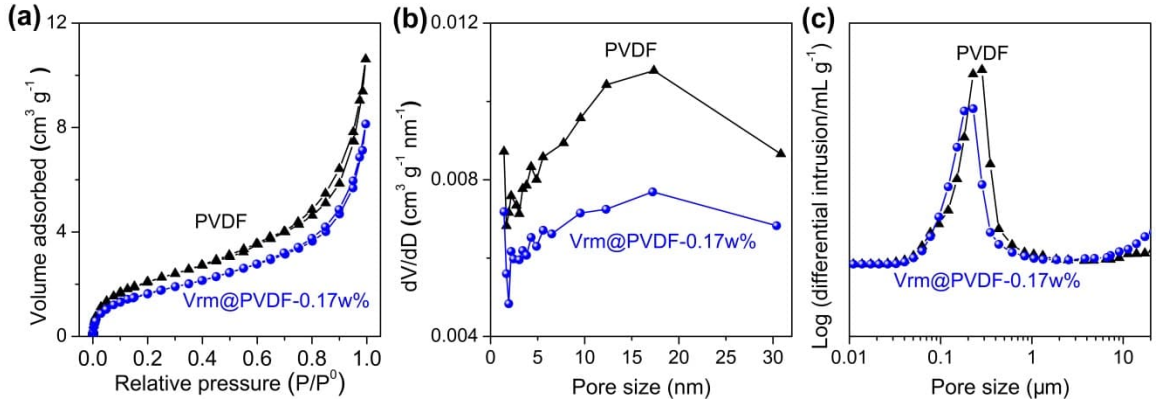

Fig. 3. (a) Nitrogen sorption isotherms and (b) corresponding pore size distribution of PVDF and Vrm@PVDF-0.17wt% porous membrane. (c) Pore size distribution of PVDF and Vrm@PVDF-0.17wt% membranes measured by the mercury intrusion porosimetry.

The selectivity of the membranes was evaluated by measuring the permeation rates of supporting electrolyte and active species in an H-cell. The diffusion curves of all membranes are linear as a whole, which conforms to the Fick diffusion law. The curves tend to be flat with time elapsing due to decreased concentration gradient. Compared with the pristine PVDF membrane, the vermiculite nanosheet modified membranes obviously reduce the diffusion of both supporting electrolyte and active species (Fig. 4a-c) due to its blocking effect. The barrier effect of nanosheets is not obvious for TEATFSI due to its small size (Fig. 4a) [36]. The permeability of $Fe(acac)_3$ is smaller than that of $Fc1N112^+$ due to its larger size [37,38]. Generally, the higher content of nanosheet (0-0.17 wt%), the slower permeation of species. Accordingly, the permeation rates of $Fc1N112^+$ and TEATFSI decrease with the vermiculite nanosheets. However, when the nanosheets content is higher than 0.17 wt%, the permeability increases, which is because the surface

of negatively charged vermiculite nanosheets can provide cation diffusion channels [29] and thus the vermiculite nanosheets can accelerate the diffusion of $FcN112^+$ and TEA^+ at high content. The ionic conductivity was measured [29], 1.17, 0.98, 0.84, 0.46 and 0.87 mS cm^{-1} for PVDF, Vrm@PVDF-0.034wt%, Vrm@PVDF-0.085wt%, Vrm@PVDF-0.17wt% and Vrm@PVDF-0.34wt%, respectively, which is well consistent with the permeability result.

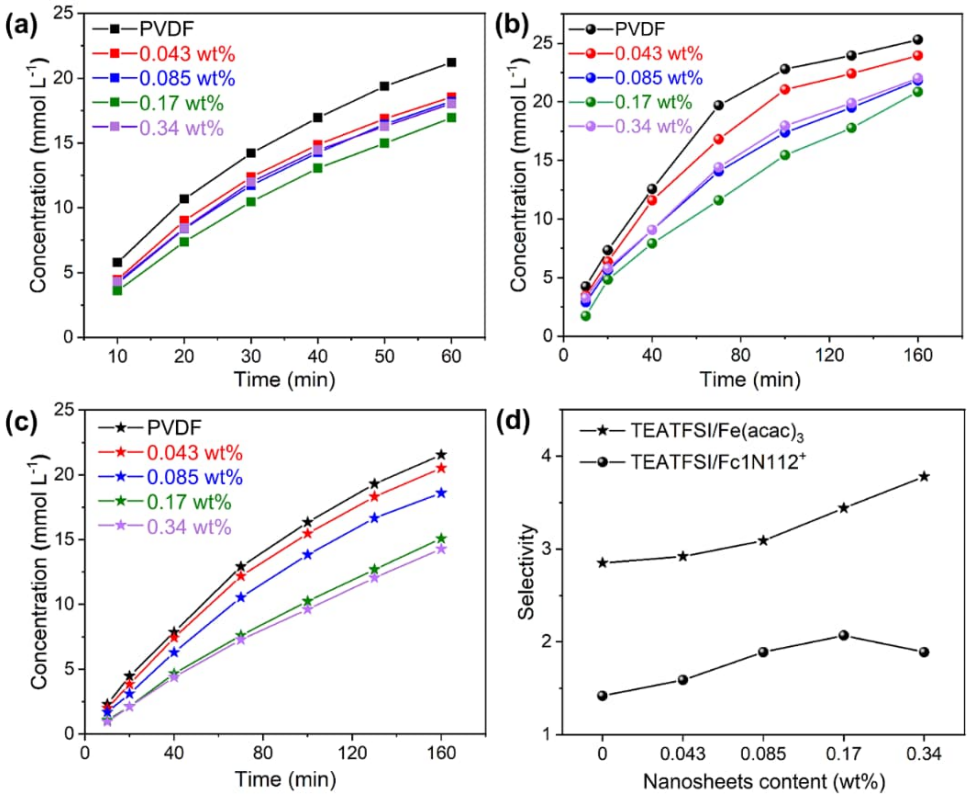

Fig. 4. Permeation rates of PVDF and Vrm@PVDF porous membrane with different contents of vermiculite nanosheets: (a) TEATFSI supporting electrolyte, (b) Fc1N112-TFSI catholyte active material, (c) $Fe(acac)_3$ anolyte active material. (d) Selectivity of PVDF and Vrm@PVDF porous membranes.

Since selectivity can evaluate the membrane performance comprehensively, the selectivity of PVDF and Vrm@PVDF membrane towards the species were calculated

(Fig. 4d). The nanosheet modified membranes show higher selectivity towards $Fc1N112^+$ and $Fe(acac)_3$. The ion selectivity increases with the content of nanosheets. The channel of membrane must be related with the content of nanosheet; it becomes more tortuous and the barrier effect becomes more obvious with increased nanosheet. In addition, the strengthened anti-swelling ability of the membranes (Fig. 2a) is helpful to alleviate the crossover effect. However, as aforementioned, the vermiculite nanosheets at high content (0.34 wt%) can enhance the diffusion of active species, resulting in higher ionic conductivity and also reduced selectivity.

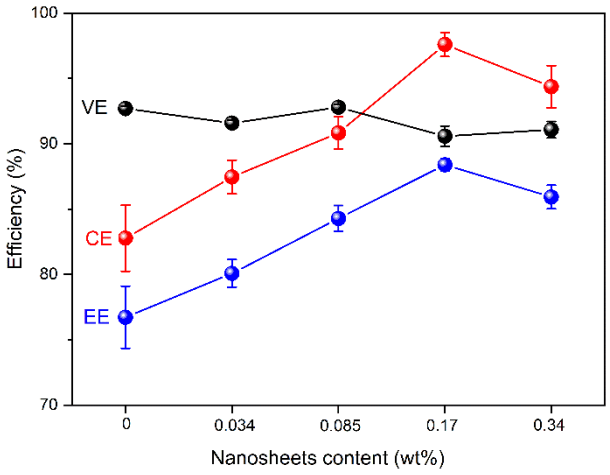

Fig. 5. Average CE, VE, and EE of Vrm@PVDF membranes as a function of vermiculite nanosheets content over 70 cycles at 2 mA cm^{-2}.

The flow cells assembled with those membranes were galvanostatically charged/discharged. As shown in Fig. 5, at 2 mA cm^{-2} for 70 cycles, the average CE and EE first increase and then decrease whereas voltage efficiency (VE) is almost constant with the content of nanosheet. Appropriate amount of vermiculite nanosheets (e.g., < 0.34%) can suppress the crossover of active species. However, excess vermiculite nanosheets can enhance the permeation rate of $Fc1N112^+$ due to cation exchange.

Correspondingly, the battery based on Vrm@PVDF-0.17wt% membrane achieves the highest CE (97.6%) and EE (88.4%), which is consistent with the trend of diffusion test. Accordingly, following discussion focuses on the Vrm@PVDF-0.17wt% membrane.

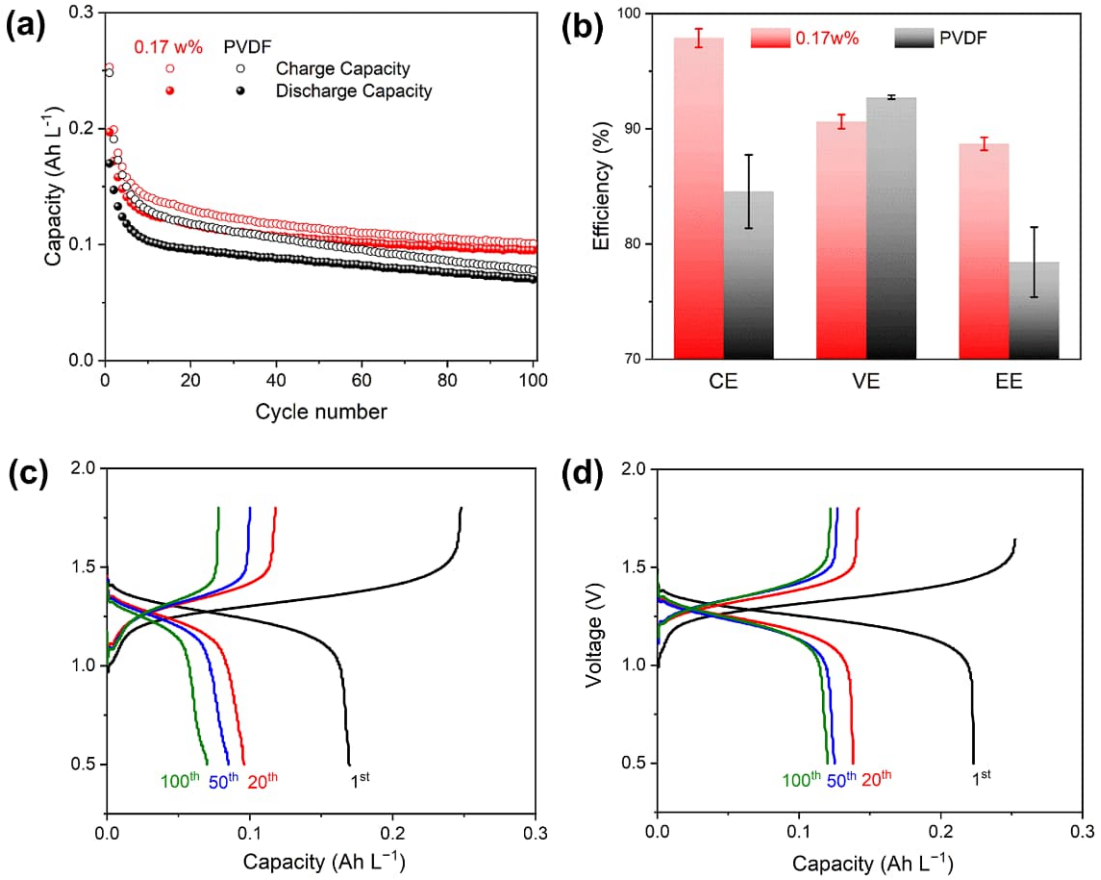

Fig. 6. (a) Cycling performance and (b) efficiency profiles of batteries with PVDF and Vrm@PVDF-0.17wt% membranes at 2 mA cm^{-2}**.** Charge/discharge curves of batteries based on (c) PVDF and (d) Vrm@PVDF-0.17wt% membranes.

In flow cell assembled with 0.01 M Fc1N112-TFSI/0.1 M TEATFSI/MeCN catholyte and 0.01 M $Fe(acac)_3$/0.1 M TEATFSI/MeCN anolyte, both PVDF and Vrm@PVDF-0.17wt% membranes can work for 100 cycles at 2 mA cm^{-2} (Fig. 6). Due to the large finger-like pores and high swelling rate, the capacity of PVDF-based battery decays rather quickly. In contrast, the Vrm@PVDF-0.17wt%-based battery operates

more stably, with average CE of 97.9%, ~16% higher than that its PVDF-based counterpart. The vermiculite nanosheets have very limited influence on VE (90.6% vs 92.7%), resulting in much higher EE (88.7% vs 78.4%). The introduction of vermiculite nanosheets significantly improves the battery discharge capacity (0.132 Ah L^{-1}), which is increased by about 50% compare with PVDF membrane (0.088 Ah L^{-1}). Furthermore, compared with that of our recent 2D vermiculite nanosheets loaded Celgard membrane-based battery [29], the present Vrm@PVDF-0.17wt% intrinsic membrane-based battery shows higher CE (97.9% vs 95.3%), VE (90.6% vs 90.1%), and discharge capacity (0.132 vs 0.104 Ah L^{-1}).

Rate performance is also one of the merits of NRFBs. The Vrm@PVDF-0.17wt% membrane–based battery can operate stably at various current densities (5~25 mA cm^{-2}, Fig. 7a and b). CE increases but VE decreases. Over the current densities studied, CE of Vrm@PVDF-0.17wt%-based battery is higher than that of PVDF-based one, especially at low current densities, e.g., 89.0% vs 71.8% at 5 mA cm^{-2}. Even at 25 mA cm^{-2}, Vrm@PVDF-0.17wt% is still advantageous, with CE of 97.8% vs 94.2%. It infers that the nanosheets can block the diffusion of active species across the membrane even at high current densities, which is different from the previous work [29].

$Fe(acac)_3$ and Fc1N112-TFSI were used as active species in this work. Their deposition on the membranes, both porous membrane and ion-exchange membrane, was found in our previous work [8,29]. In this work, however, no deposition of active species is found, as evidenced by the almost constant ohmic resistance (dominated by the film resistance) of the batteries before and after cycling tests (Fig. 7c and d). The addition of nanosheets only increases the film resistance slightly (3.8 vs 3.3 Ω cm^2). It is probably

due to the swelling property of the PVDF-based intrinsic membrane [39]. Generally, the intrinsic membranes show higher swelling in organic solvent, which facilitates the diffusion of the molecules. Accordingly, the deposition of active species on the membranes is significantly alleviated and thus lower resistance.

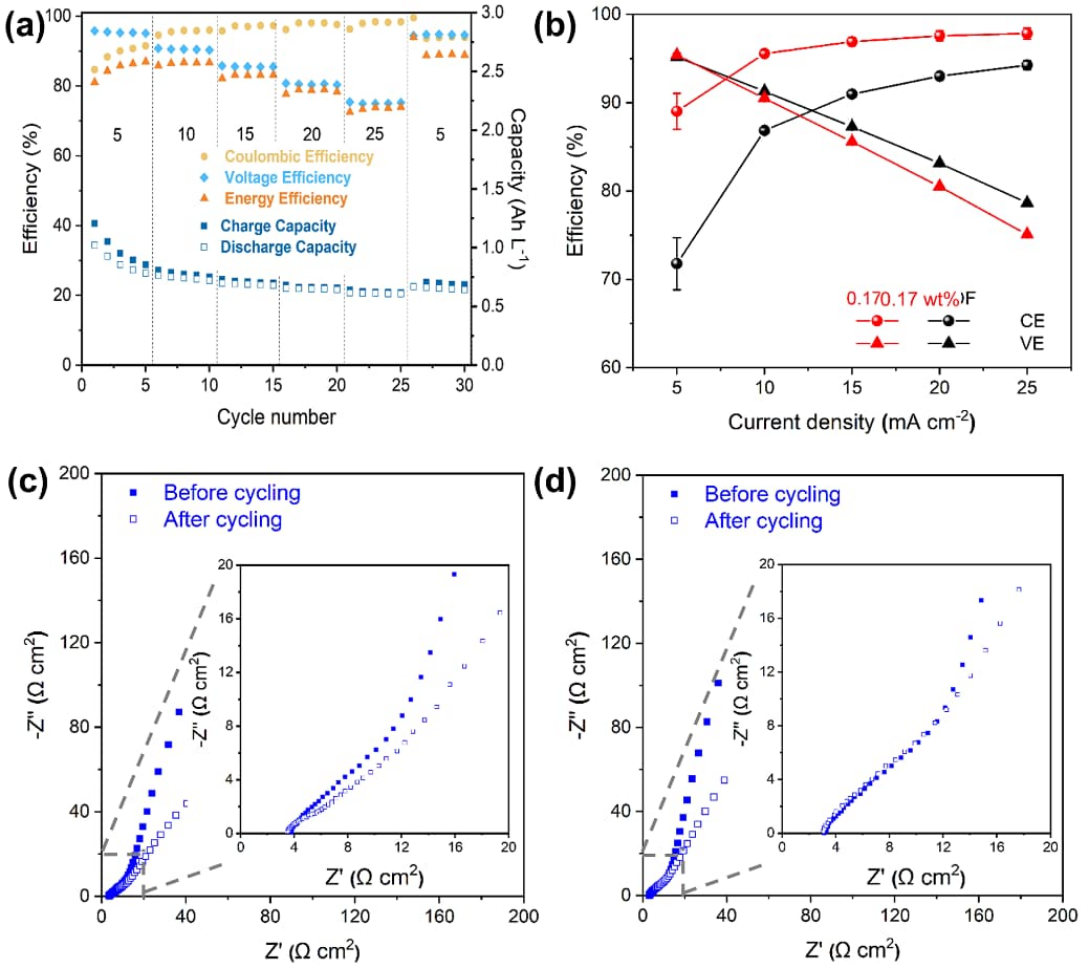

Fig. 7. (a) Rate capability of Vrm@PVDF-0.17wt% membrane-based battery. (b) Average CE and VE of the batteries with PVDF and Vrm@PVDF-0.17wt% membranes at different current densities. EIS of fresh and cycled (c) Vrm@PVDF-0.17wt% and (d) PVDF membranes.

The performance of Vrm@PVDF-0.17wt% membrane-based battery with high-concentration electrolyte (0.05 M Fc1N112-TFSI/0.5 M TEATFSI catholyte and 0.05 M $Fe(acac)_3$/0.5 M TEATFSI anolyte) was further examined. It can operate fairly stable at 10 mA cm^{-2} over 100 cycles without the deposition of active species (Fig. 8). It yields average CE of 96.1%, VE of 90.0%, EE of 86.5% and discharge capacity of 0.64 Ah L^{-1}, which outperform many NARFBs based on commercial porous membranes (Table 1).

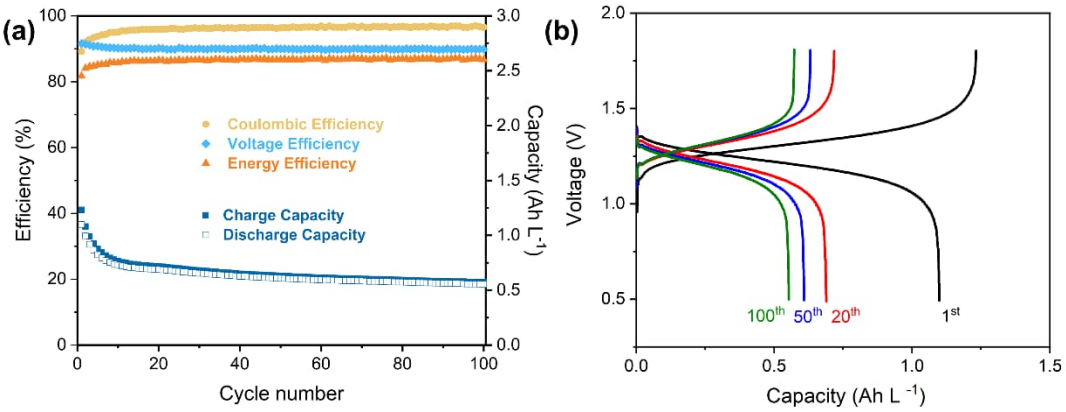

Fig. 8. (a) Cycling performance and (b) charge/discharge curves at selected cycles of cell with Vrm@PVDF-0.17wt% membrane at 10 mA cm^{-2}.

Table 1. Performance comparison of NARFBs with commercial porous membranes.

Electrolyte	Membrane	*j* (mA cm^{-2})	Cycles	CE (%)	VE (%)	EE (%)	Ref.
0.01 M Fc1N112-TFSI/$Fe(acac)_3$	Vrm@PVDF	2	100	97.9	90.6	88.6	This
0.05 M Fc1N112-TFSI/$Fe(acac)_3$	Vrm@PVDF	10	100	96.1	90.0	86.5	work
0.3 M DBMMB/MePh	Daramic 175	35	50	90	77	69	[40]
0.1 M Fc1N112-TFSI/$Fe(acac)_3$	Daramic 250	10	100	88.3	91.6	81.1	[8]
0.1 M DBMMB/BzNSN	Daramic 800	10	100	94	77	72	[41]
0.1 M $FeCp_2PPh_2RCN$/Li	Celgard 2325	10	60	98	–	78	[42]
0.01 M $V(acac)_3$	Celgard 2400	1.39	10	49	–	32	[43]
0.05 M DBPZ/0.1 M FL	Celgard 4560	20	30	90	78	70	[44]

4. Conclusions

The porous PVDF membrane with 2D vermiculite nanosheets modification is proposed and prepared for NARFB. The vermiculite nanosheets effectively reduce the swelling rate, increase the mechanical strength and ion selectivity of the membrane. The battery with the new Vrm@PVDF membrane exhibits higher CE (97.9% vs 84.6%) and larger average capacity (0.132 vs 0.088 Ah L^{-1}) compared with its pristine PVDF counterpart at 2 mA cm^{-2}. The vermiculite nanosheets have little effect on VE (90.6% vs 92.7%). The porous structure of Vrm@PVDF membrane enables high-rate operation, with CE of 97.8% and EE of 75.1% at 25 mA cm^{-2}. The battery with such Vrm@PVDF membrane shows comparable and even superior performance than that with commercial porous and ion exchange membranes, which sheds light on the development of high-performance membranes for NARFBs.

Acknowledgements

The work was financially supported by the National Natural Science Foundation of China (21636007).

References

[1] R. Ye, D. Henkensmeier, S.J. Yoon, Z. Huang, D.K. Kim, Z. Chang, S. Kim, R. Chen, Redox flow batteries for energy storage: A technology review, J. Electrochem. Energy Convers. Storage 15 (2018) 010801. https://doi.org/10.1115/1.4037248.

[2] Y. Yao, J. Lei, Y. Shi, F. Ai, Y. Lu, Assessment methods and performance metrics for redox flow batteries, Nat. Energy 6 (2021) 582-588. https://doi.org/10.1038/s41560-020-00772-8.

[3] K. Gong, Q. Fang, S. Gu, S. Li, Y. Yan, Nonaqueous redox-flow batteries: organic solvents, supporting electrolytes, and redox pairs, Energy Environ. Sci. 8 (2015) 3515-

3530. https://doi.org/10.1039/c5ee02341f.

[4] Y. Matsuda, K. Tanaka, M. Okada, Y. Takasu, M. Morita, T.J.J.o.A.E. Matsumura-Inoue, A rechargeable redox battery utilizing ruthenium complexes with non-aqueous organic electrolyte, J. Appl. Electrochem. 18 (1988) 909-914. https://doi.org/10.1007/BF01016050.

[5] P. Leung, A.A. Shah, L. Sanz, C. Flox, J.R. Morante, Q. Xu, M.R. Mohamed, C.P. de Leon, F.C. Walsh, Recent developments in organic redox flow batteries: A critical review, J. Power Sources 360 (2017) 243-283. https://doi.org/10.1016/j.jpowsour.2017.05.057.

[6] J. Yuan, Z. Pan, Y. Jin, Q. Qiu, C. Zhang, Y. Zhao, Y. Li, Membranes in non-aqueous redox flow battery: A review, J. Power Sources 500 (2021) 229983. https://doi.org/10.1016/j.jpowsour.2021.229983.

[7] C.S. Sevov, S.L. Fisher, L.T. Thompson, M.S.J.J.o.t.A.C.S. Sanford, Mechanism-based development of a low-potential, soluble, and cyclable multielectron anolyte for nonaqueous redox flow batteries, J. Am. Chem. Soc. 138 (2016) 15378-15384. https://doi.org/10.1021/jacs.6b07638.

[8] Y. Zhen, C. Zhang, J. Yuan, Y. Zhao, Y. Li, A high-performance all-iron non-aqueous redox flow battery, J. Power Sources 445 (2020) 227331. https://doi.org/10.1016/j.jpowsour.2019.227331.

[9] Z. Li, Y. Lu, Polysulfide-based redox flow batteries with long life and low levelized cost enabled by charge-reinforced ion-selective membranes, Nat. Energy 6 (2021) 517-528. https://doi.org/10.1038/s41560-021-00804-x.

[10] H. Zhang, H. Zhang, X. Li, Z. Mai, J. Zhang, Nanofiltration (NF) membranes: the next generation separators for all vanadium redox flow batteries (VRBs)?, Energy

Environ. Sci. 4 (2011) 1676-1679. https://doi.org/10.1039/c1ee01117k.

[11] H. Zhang, H. Zhang, X. Li, Z. Mai, W. Wei, Silica modified nanofiltration membranes with improved selectivity for redox flow battery application, Energy Environ. Sci. 5 (2012) 6299-6303. https://doi.org/10.1039/c1ee02571f.

[12] X. Che, H. Zhao, X. Ren, D. Zhang, H. Wei, J. Liu, X. Zhang, J. Yang, Porous polybenzimidazole membranes with high ion selectivity for the vanadium redox flow battery, J. Membr. Sci. 611 (2020) 118359. https://doi.org/10.1016/j.memsci.2020.118359.

[13] K.H. Hendriks, S.G. Robinson, M.N. Braten, C.S. Sevov, B.A. Helms, M.S. Sigman, S.D. Minteer, M.S. Sanford, High-performance oligomeric catholytes for effective macromolecular separation in nonaqueous redox flow batteries, ACS Cent. Sci. 4 (2018) 189-196. https://doi.org/10.1021/acscentsci.7b00544.

[14] L. Fu, N.A. Hashim, Y. Liu, M. Abed, K. Li, Progress in the production and modification of PVDF membranes, J. Membr. Sci. 375 (2011) 1-27. https://doi.org/10.1016/j.memsci.2011.03.014.

[15] T.A. Otitoju, A.L. Ahmad, B.S. Ooi, Polyvinylidene fluoride (PVDF) membrane for oil rejection from oily wastewater: A performance review, J. Water Process. Eng. 14 (2016) 41-59. https://doi.org/10.1016/j.jwpe.2016.10.011.

[16] S.S. Madaeni, M.K. Yeganeh, Microfiltration of emulsified oil wastewater, J. Porous Mat. 10 (2003) 131-138. https://doi.org/10.1023/A:1026035830187.

[17] W. Wei, H. Zhang, X. Li, H. Zhang, Y. Li, I. Vankelecom, Hydrophobic asymmetric ultrafiltration PVDF membranes: an alternative separator for VFB with excellent stability, Phys. Chem. Chem. Phys. 15 (2013) 1766-1771. https://doi.org/10.1039/c2cp43761a.

[18] W. Lu, Z. Yuan, Y. Zhao, H. Zhang, X. Li. Porous membranes in secondary battery technologies, Chem. Soc. Rev. 46 (2017) 2199-2236. https://doi.org/10.1039/c6cs00823b.

[19] X. Lou, J. Ye, L. Xia, S. Chang, X. Zhao, C. Wu, M. Ding, Highly efficient and low cost SPEEK/TiO_2 nanocomposite membrane for vanadium redox flow battery, J. Nanosci. Nanotechnol. 19 (2019) 2247-2252. https://doi.org/10.1166/jnn.2019.16467.

[20] M.M. Seepana, J. Pandey, A. Shukla, Design and synthesis of highly stable poly(tetrafluoroethylene)-zirconium phosphate (PTFE-ZrP) ion-exchange membrane for vanadium redox flow battery (VRFB), Ionics 23 (2017) 1471-1480. https://doi.org/10.1007/s11581-016-1967-8.

[21] Z. Yuan, X. Zhu, M. Li, W. Lu, X. Li, H. Zhang, A highly ion-selective zeolite flake layer on porous membranes for flow battery applications, Angew. Chem. Int. Ed. Engl. 55 (2016) 3058-3062. https://doi.org/10.1002/anie.201510849.

[22] J. Yuan, C. Zhang, T. Liu, Y. Zhen, Z. Pan, Y. Li, Two-dimensional metal-organic framework nanosheets-modified porous separator for non-aqueous redox flow batteries, J. Membr. Sci. 612 (2020) 118463. https://doi.org/10.1016/j.memsci.2020.118463.

[23] Y. Heo, H. Im, J. Kim, The effect of sulfonated graphene oxide on sulfonated poly (ether ether ketone) membrane for direct methanol fuel cells, J. Membr. Sci. 425 (2013) 11-22. https://doi.org/10.1016/j.memsci.2012.09.019.

[24] J. Li, Y. Zhang, S. Zhang, X. Huang, Sulfonated polyimide/s-MoS_2 composite membrane with high proton selectivity and good stability for vanadium redox flow battery, J. Membr. Sci. 490 (2015) 179-189. https://doi.org/10.1016/j.memsci.2015.04.053.

[25] Y. Zhang, Y. Pu, P. Yang, H. Yang, S. Xuan, J. Long, Y. Wang, H. Zhang, Branched

sulfonated polyimide/functionalized silicon carbide composite membranes with improved chemical stabilities and proton selectivities for vanadium redox flow battery application, J. Membr. Sci. 53 (2018) 14506-14524. https://doi.org/10.1007/s10853-018-2620-x.

[26] F. Jia, S.Song, Exfoliation and characterization of layered silicate minerals: A review, Surf. Rev. Lett. 21 (2014) 1430001. https://doi.org/10.1142/S0218625X14300019.

[27] R. Xu, Y. Sun, Y. Wang, J. Huang, Q. Zhang, Two-dimensional vermiculite separator for lithium sulfur batteries, Chin. Chem. Lett. 28 (2017) 2235-2238. https://doi.org/10.1016/j.cclet.2017.09.065.

[28] W. Tang, S. Tang, C. Zhang, Q. Ma, Q. Xiang, Y. Yang, J. Luo, Simultaneously enhancing the thermal stability, mechanical modulus, and electrochemical performance of solid polymer electrolytes by incorporating 2D sheets, Adv. Energy Mater. 8 (2018) 1800186. https://doi.org/10.1002/aenm.201800866.

[29] T. Liu, C. Zhang, J. Yuan, Y. Zhen, Y. Li, Two-dimensional vermiculite nanosheets-modified porous membrane for non-aqueous redox flow batteries, J. Power Sources 500 (2021) 229987. https://doi.org/10.1016/j.jpowsour.2021.229987.

[30] X. Wei, L. Cosimbescu, W. Xu, J. Hu, M. Vijayakumar, J. Feng, M. Hu, X. Deng, J. Xiao, J. Liu, V. Sprenkle, W. Wang, Towards high-performance nonaqueous redox flow electrolyte via ionic modification of active species, Adv. Energy Mater. 5 (2015) 1400678. https://doi.org/10.1002/aenm.201400678.

[31] L. Timperman, P. Skowron, A. Boisset, H. Galiano, D. Lemordant, E. Frackowiak, F. Beguin, M. Anouti, Triethylammonium bis(tetrafluoromethylsulfonyl)amide protic ionic liquid as an electrolyte for electrical double-layer capacitors, Phys. Chem. Chem. Phys.

14 (2012) 8199-8207. https://doi.org/10.1039/c2cp40315c.

[32] C. Wu, H. Bai, Y. Lv, Z. Lv, Y. Xiang, S. Lu, Enhanced membrane ion selectivity by incorporating graphene oxide nanosheet for vanadium redox flow battery application, Electrochim. Acta 248 (2017) 454-461. https://doi.org/10.1016/j.electacta.2017.07.122.

[33] W. Tian, Z. Li, Z. Ge, D. Xu, K. Zhang, Self-assembly of vermiculite-polymer composite films with improved mechanical and gas barrier properties, Appl. Clay Sci. 180 (2019) 105198. https://doi.org/10.1016/j.clay.2019.105198.

[34] A.D. Macheca, W.W. Focke, H.F. Muiambo, M. Kaci, Stiffening mechanisms in vermiculite-amorphous polyamide bio-nanocomposites, Eur. Polym. J. 74 (2016) 51-63. https://doi.org/10.1016/j.eurpolymj.2015.11.013.

[35] P. Demontis, M. Masia, G.B. Suffritti, Peculiar structure of water in slightly superhydrated vermiculite clay studied by car-parrinello molecular dynamics simulations, J. Phys. Chem. C 118 (2014) 7923-7931. https://doi.org/10.1021/jp409723x.

[36] M. Ue, Mobility and ionic association of lithium and quaternary ammonium salts in propylene carbonate and γ-butyrolactone, J. Electrochem. Soc. 141 (1994) 3336-3342. https://doi.org/10.1149/1.2059336.

[37] M. Hu, Z. Jin, Q. Miao, L. Fang, Crystal structure of tris(acetylacetonato)iron(III), $C_{15}H_{21}O_6Fe$, at 20 K, Z. Krist.-New Cryst. Struct. 216 (2001) 597-598. https://doi.org/10.1524/ncrs.2001.216.14.631.

[38] K. Han, N.N. Rajput, X. Wei, W. Wang, J. Hu, K.A. Persson, K.T. Mueller, Diffusional motion of redox centers in carbonate electrolytes, J. Chem. Phys. 141 (2014) 104509. https://doi.org/10.1063/1.4894481.

[39] J. Saunier, F. Alloin, J.Y. Sanchez, R. Barrière, Plasticized microporous

poly(vinylidene fluoride) separators for lithium-ion batteries. II. Poly(vinylidene fluoride) dense membrane swelling behavior in a liquid electrolyte - Characterization of the swelling kinetics, J. Polym. Sci. Part B: Polym. Lett. 43 (2004) 544-552. https://doi.org/10.1002/polb.10729.

[40] X. Wei, W. Duan, J. Huang, L. Zhang, B. Li, D. Reed, W. Xu, V. Sprenkle, W. Wang, A high-current, stable nonaqueous organic redox flow battery, ACS Energy Lett. 1 (2016) 705-711. https://doi.org/10.1021/acsenergylett.6b00255.

[41] J. Yuan, C. Zhang, Y. Zhen, Y. Zhao, Y. Li, Enhancing the performance of an all-organic non-aqueous redox flow battery, J. Power Sources 443 (2019) 227283. https://doi.org/ 10.1016/j.jpowsour.2019.227283.

[42] C. Xie, W. Xu, H. Zhang, X. Hu, X. Li, A multi-electron transfer ferrocene derivative positive redox moiety with improved solubility and potential, Chem. Commun. 54 (2018) 8419-8422. https://doi.org/10.1039/c8cc04099k.

[43] H.S. Bang, D. Kim, S.S. Hwang, J. Won, Surface-modified porous membranes with electrospun Nafion/PVA fibres for non-aqueous redox flow battery, J. Membr. Sci. 514 (2016) 186-194. https://doi.org/10.1016/j.memsci.2016.04.068.

[44] G. Kwon, S. Lee, J. Hwang, H.-S. Shim, B. Lee, M.H. Lee, Y. Ko, S.-K. Jung, K. Ku, J. Hong, K. Kang, Multi-redox molecule for high-energy redox flow batteries, Joule 2 (2018) 1771-1782. https://doi.org/10.1016/j.joule.2018.05.014.